AGU PUBLICATIONS

Geophysical Research Letters

RESEARCH LETTER
10.1002/2016GL070565

Key Points:
- Surface and subsurface chlorophyll maxima are connected along isopycnals
- Chlorophyll transport is consistent with down-gradient potential vorticity flux
- Model results confirm mean and eddy pathways for DCM formation

Supporting Information:
- Supporting Information S1
- Movie S1

Correspondence to:
Z. K. Erickson,
zerickso@caltech.edu

Citation:
Erickson, Z. K., A. F. Thompson, N. Cassar, J. Sprintall, and M. R. Mazloff (2016), An advective mechanism for deep chlorophyll maxima formation in southern Drake Passage, *Geophys. Res. Lett.*, *43*, 10,846–10,855, doi:10.1002/2016GL070565.

Received 3 AUG 2016
Accepted 28 SEP 2016
Accepted article online 3 OCT 2016
Published online 18 OCT 2016

An advective mechanism for deep chlorophyll maxima formation in southern Drake Passage

Zachary K. Erickson[1], Andrew F. Thompson[1], Nicolas Cassar[2], Janet Sprintall[3], and Matthew R. Mazloff[3]

[1] Environmental Science and Engineering, California Institute of Technology, Pasadena, California, USA, [2] Division of Earth and Ocean Sciences, Nicholas School of the Environment, Duke University, Durham, North Carolina, USA, [3] Scripps Institution of Oceanography, La Jolla, California, USA

Abstract We observe surface and subsurface fluorescence-derived chlorophyll maxima in southern Drake Passage during austral summer. Backscatter measurements indicate that the deep chlorophyll maxima (DCMs) are also deep biomass maxima, and euphotic depth estimates show that they lie below the euphotic layer. Subsurface, offshore and near-surface, onshore features lie along the same isopycnal, suggesting advective generation of DCMs. Temperature measurements indicate a warming of surface waters throughout austral summer, capping the winter water (WW) layer and increasing off-shelf stratification in this isopycnal layer. The outcrop position of the WW isopycnal layer shifts onshore, into a surface phytoplankton bloom. A lateral potential vorticity (PV) gradient develops, such that a down-gradient PV flux is consistent with offshore, along-isopycnal tracer transport. Model results are consistent with this mechanism. Subduction of chlorophyll and biomass along isopycnals represents a biological term not observed by surface satellite measurements which may contribute significantly to the strength of the biological pump in this region.

1. Introduction

The oceans account for approximately half of global photosynthesis [*Field et al.*, 1998], yet productivity estimates are poorly constrained [*Carr et al.*, 2006]. High-latitude regions ventilate the deep ocean and contribute to carbon sequestration on long time scales [*Sarmiento and Toggweiler*, 1984; *Martin*, 1990; *Broecker et al.*, 1998]. High-nutrient low-chlorophyll (HNLC) conditions prevail over much of the Southern Ocean, where primary production is thought to be limited by the availability of iron and light [*Martin*, 1990; *Boyd and Ellwood*, 2010; *Cassar et al.*, 2011]. The Southern Ocean is a source region for nonanthropogenic carbon dioxide due to inefficient photosynthesis [*Gruber et al.*, 2009]. Locally, however, convergence of micronutrients can lead to large chlorophyll blooms [*Measures et al.*, 2013; *Frants et al.*, 2013].

Deep chlorophyll maxima (DCMs) are an important component of the biological pump, accounting in some cases for over half of depth-integrated primary production and export production [*Hood et al.*, 1991; *Weston et al.*, 2005; *Omand et al.*, 2015]. DCMs are generally considered in a one-dimensional framework [*Cullen*, 2015], where they have been attributed to photoacclimation processes [*Cullen*, 1982; *Neori et al.*, 1984; *Longhurst and Harrison*, 1989]; formation of thin phytoplankton layers driven by straining processes, vertical migration, and buoyancy control [*Ralston et al.*, 2007; *Richardson and Cullen*, 1995; *Stacey et al.*, 2007]; and subsurface production maxima caused by colimitation of photosynthesis by light and nutrients [*Mitchell et al.*, 1991; *Holm-Hansen and Mitchell*, 1991]. *Holm-Hansen and Hewes* [2004] studied these features in the Western Antarctic Peninsula (WAP) region in southern Drake Passage and found evidence of a persistent DCM. They suggested that the bloom was sustained by in situ biological growth and linked biological production to an observed increase in oxygen concentration at the depth of the DCM.

In contrast, other studies have pointed to allochthonous origins of DCMs through subduction of water masses. *Hood et al.* [1991], *Kadko et al.* [1991], and *Washburn et al.* [1991] used ship-based observations to show subduction of biomass along isopycnals in narrow filaments off the coast of California. The subducted features were high in chlorophyll concentration but located beneath the euphotic layer [*Hood et al.*, 1991; *Washburn et al.*, 1991]. Particle size distributions [*Hood et al.*, 1991] and radium isotope measurements [*Kadko et al.*, 1991] both indicated that the subducted features had been produced over a time period of hours to days.

Recently, *Omand et al.* [2015] found strong evidence of eddy-driven subduction of particulate organic carbon along isopycnals in the North Atlantic and estimated that this process may account for half of the total biological export in the Southern Ocean. Model results from this study highlighted the importance of submesoscale (1–10 km) dynamics in these subduction events.

Along-isopycnal subduction can be broken into submesoscale ageostrophic and mesoscale geostrophic components. Fronts at the submesoscale induce an ageostrophic circulation with associated vertical velocities of tens of meters per day [*Lapeyre et al.*, 2006; *Mahadevan and Tandon*, 2006; *Levy et al.*, 2012; *Rosso et al.*, 2014]. At larger scales, mesoscale eddies mix properties along isopycnals. Eddies are generated in frontal systems and are ubiquitous in the Drake Passage region [*Frenger et al.*, 2015].

Here we use ocean glider observations to show the development of a DCM in southern Drake Passage. We provide evidence that this development is affected by physical processes and propose a mechanism by which eddy mass fluxes associated with a potential vorticity (PV) gradient subduct surface waters with high chlorophyll and/or high micronutrient concentrations. Our data and methods are given in section 2. Results are summarized in section 3, and a discussion and conclusions are in sections 4 and 5.

2. Data and Methods

2.1. Deployment Site

Drake Passage is a choke point in the Southern Ocean, where the Antarctic Circumpolar Current (ACC) funnels through a gap of only 800 km, leading to high-velocity shear, strong frontal systems, and a vigorous eddy field. The continental slope generates persistent, topographically steered fronts along the southern boundary, similar to other areas of the Southern Ocean such as the Kerguelen and Campbell Plateaus [*Zhou et al.*, 2010; *Sokolov and Rintoul*, 2009; *Thompson et al.*, 2010; *Rosso et al.*, 2015; *Frenger et al.*, 2015].

Our study area is in southern Drake Passage, upstream of the Shackleton Fracture Zone (SFZ; Figure 1a). This region contains the Southern Boundary of the ACC (SBACC) and the Southern ACC Front [*Orsi et al.*, 1995; *Sokolov and Rintoul*, 2009], which are strongly steered by topography [*Zhou et al.*, 2010], being channeled through the Shackleton Gap and northward around the SFZ, respectively. A surface bloom in this area occurs in austral summer and is associated with the shelf break [*Holm-Hansen et al.*, 2005]. This area is one of the major HNLC regions, where growth is thought to be colimited by light and iron [*Martin et al.*, 1990; *Dulaiova et al.*, 2009], and is upstream from the highly productive Scotia Sea. Waters sourced from the shelf or nearby Bransfield Strait may supply crucial micronutrients to the region [*Measures et al.*, 2013].

2.2. Seaglider Data

We use 3 months of high-resolution data from an autonomous, buoyancy-driven Seaglider during austral summer (December 2014 to March 2015) as part of the ChinStrAP (Changes in Stratification at the Antarctic Peninsula) project. The glider followed a sawtooth pattern to 1000 m depth, with average spacing between dives of 3–5 km. Measurements were taken of temperature (T), salinity (S), and pressure (p) with a Sea-Bird CTD Sail, oxygen (O_2) with an Aanderaa optode, and fluorescence (F), backscatter (b_{bp}) at 650 nm, and CDOM (colored dissolved organic matter) with a WETLabs ECOPuck Triplet.

Fluorescence is a widely used proxy for chlorophyll *a* (Chl) and, often, for phytoplankton biomass. The scale factor relating fluorescence and chlorophyll concentration (F:Chl) was determined in a factory calibration with a *Thalassiosira weissflogii* diatom monoculture. This scale factor is highly dependent on a range of factors, including community composition and structure [*Cullen*, 1982; *Boss et al.*, 2008] and nutrient and light stress [*Slovacek and Hannan*, 1977; *Neori et al.*, 1984], which can vary over small spatial and temporal scales [*Cullen*, 1982; *Boss et al.*, 2008]. We compared nighttime surface fluorescence-derived chlorophyll measurements to remotely sensed chlorophyll concentrations from Moderate Resolution Imaging Spectroradiometer (MODIS) Aqua and found good agreement with the factory calibration (supporting information Figure S1).

During daytime, the ratio F:Chl decreases at the surface due to an array of photoadaptative processes collectively known as nonphotochemical quenching (NPQ) [*Cullen and Lewis*, 1995]. A common NPQ correction relies on a constant ratio between backscatter and fluorescence measurements below the surface in the mixed layer [*Boss et al.*, 2008; *Boss and Haëntjens*, 2016]. This method was used to generate our "NPQ-corrected chlorophyll" results.

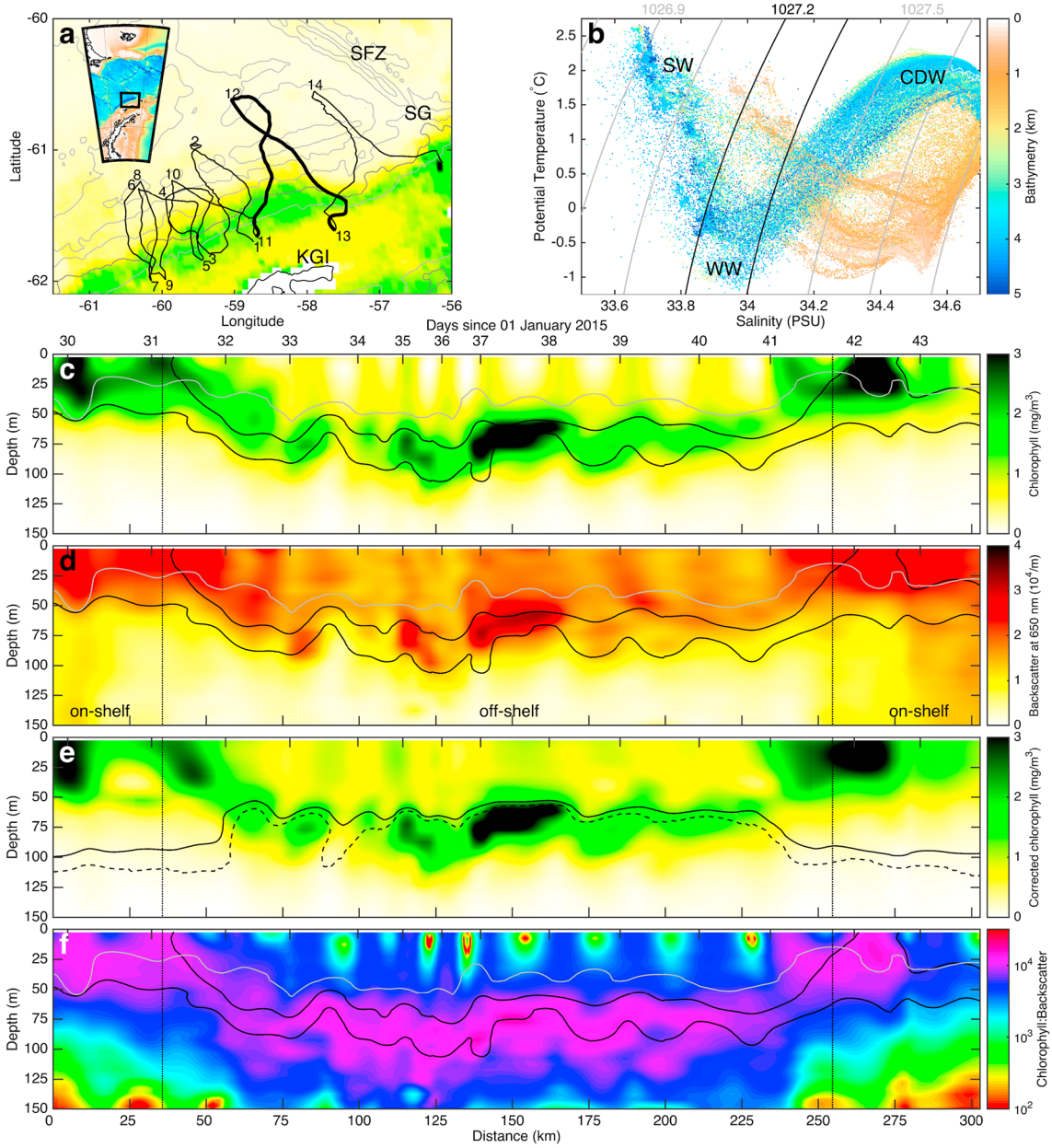

Figure 1. Overview of the study region. (a) Average satellite chlorophyll (5 December 2014 to 2 March 2015) from MODIS Aqua, using the *Johnson et al.* [2013] algorithm with colorbar as in Figure 1c, with bathymetry contours every 1 km (grey) and glider transects (black). Inset shows the region in a larger context with bathymetry colorbar as in Figure 1b. Shackleton Fracture Zone (SFZ), Shackleton Gap (SG), and King George Island (KGI; black contour) are labeled. (b) Temperature-salinity plot of Transects 1–14; colors denote bathymetry. Circumpolar Deep Water (CDW), winter water (WW), and surface waters (SW) are labeled, and isopycnal contours (kg/m^3) are overlain in grey and black. (c) Objectively mapped chlorophyll, (d) backscatter, (e) corrected chlorophyll, and (f) the chlorophyll:backscatter ratio from Transects 11 and 12 (bold line in Figure 1a). Isopycnal contours at 1027.2 and 1027.35 kg/m^3 in black are shown in Figures 1b–1d, and 1f. Mixed layer depth is given in grey in Figures 1c, 1d, and 1f. Black solid (dashed) line in Figure 1e gives the euphotic depth, defined as the 1% light level (0.1 mol/m^2/day isolume). Dotted vertical black lines in Figures 1c–1f give the location of the 2000 m isobath.

More information on the processing, calibration, and NPQ correction methods are given in Supporting Information S1. We note that in situ calibration steps during the bloom were not available due to the autonomous nature of our sampling and emphasize that our results are primarily dependent on the relative spatial and temporal distribution of the Chl or biomass concentrations as opposed to their absolute values.

2.3. Mixed Layer Depth Calculations

We calculate the mixed layer depth (MLD) as the depth at which the potential density differs by a threshold value of 0.03 kg/m^3 from the potential density at 10 m depth [*Dong et al.*, 2008].

2.4. Euphotic Depth Calculation

We adapt the method given in *Arrigo et al.* [2008] to estimate the propagation of photosynthetically available radiation (PAR; 400–700 nm) through the water column. Our approach differs from that of *Arrigo et al.* [2008] in that we use depth-resolved glider chlorophyll concentrations, ozone measurements from NASA OMI (Ozone Monitoring Instrument), sea level pressure and wind data from the Antarctic Mesoscale Prediction System (AMPS), and choose a relatively clear visibility of 12 km. We use the NPQ-corrected chlorophyll results to estimate light propagation during daytime measurements.

The euphotic depth is often taken as the depth at which 1% of surface PAR is available [e.g., *Ryther*, 1956; *Behrenfeld and Falkowski*, 1997; *Dunne et al.*, 2005]. Because phytoplankton respond to absolute rather than relative light levels, the 1% PAR threshold may not be the best measure of the euphotic depth [*Banse*, 2004]. *Holm-Hansen and Mitchell* [1991] estimate the euphotic depth in this region at approximately the 0.1 mol quanta/m^2/day isolume. We estimate this depth by correcting solar irradiance for cloud cover as in *Arrigo et al.* [2008] using daily averaged AMPS cloud fraction and calculating daily insolation from hourly estimates of PAR.

2.5. Satellite Measurements

We include in our analysis satellite observations of surface chlorophyll from the MODIS Aqua platform at 4 km resolution using the *Johnson et al.* [2013] algorithm. This method updates the reflectance ratio coefficients using only Southern Ocean measurements, showing substantially larger amounts of chlorophyll in the Southern Ocean than the standard global algorithms [*Mitchell and Holm-Hansen*, 1991; *Kahru and Mitchell*, 2010]. We temporally average the results by taking the mean value over all days with valid observations. Satellite imagery produces values representative of ocean conditions within about one optical depth of the surface, which for 550 nm light is approximately 20 m [*Gordon and McCluney*, 1975] but can be highly dependent on seawater constituents [*Arrigo et al.*, 1998].

2.6. Southern Ocean Model

To test the advective hypothesis, a 1/12° simulation of the Southern Ocean was run using the MITgcm [*Marshall et al.*, 1997]. The domain is 78°S to the equator, with lower resolution north of 30°S. Topography is prescribed using ETOPO1 [*Amante and Eakins*, 2009]. The model has 104 vertical levels with partial bottom cells. An atmospheric boundary layer scheme is employed where fluxes of heat, freshwater (salt), and momentum are determined by bulk formulae [*Large and Yeager*, 2004]. The atmospheric state is prescribed from the ERA-Interim reanalysis. Runoff is prescribed at the continental boundary. Initial conditions are derived from a 1/6° Southern Ocean state estimate [*Mazloff et al.*, 2010]. The model is run from 2005 to 2010, with a 1 year spin-up to the increased resolution. We analyze model results from austral summer 2008–2009, but our analysis is not strongly dependent on the year considered.

3. Results

We consider 14 glider transects that are roughly perpendicular to bathymetric contours (Figure 1a and Table S1). We define glider dives as being south (onshore) or north (offshore) of the SBACC, which is well approximated by the 2000 m isobath. This isobath is also the approximate limit of the surface phytoplankton bloom, as shown by satellite measurements (Figure S4). Temperature/salinity properties in our area show the presence of a strong frontal system associated with the SBACC (Figure 1b).

3.1. Chlorophyll Distribution

The vertical distribution of fluorescence tracks the growth of both an on-shelf surface-intensified chlorophyll bloom and a DCM. Interpolated chlorophyll data for Transects 11 and 12 are shown in Figure 1c (all transects in Figure S5). The on-shelf bloom is coincident with the chlorophyll levels observed from satellite. This bloom reaches approximately 50 m depth and is bounded by the mixed layer.

The DCM develops soon after the surface bloom and is of a similar magnitude but centered beneath the mixed layer at 50–90 m depth. It lies along the same isopycnal as the surface bloom (black lines in Figure 1c) and, importantly, is not found until after the surface bloom is expressed and the isopycnal layer outcrop location migrates onto the shelf (Figure S5, Transect 5). An off-shelf bloom is not shown in satellite observations at any point throughout the glider deployment (Figure S4).

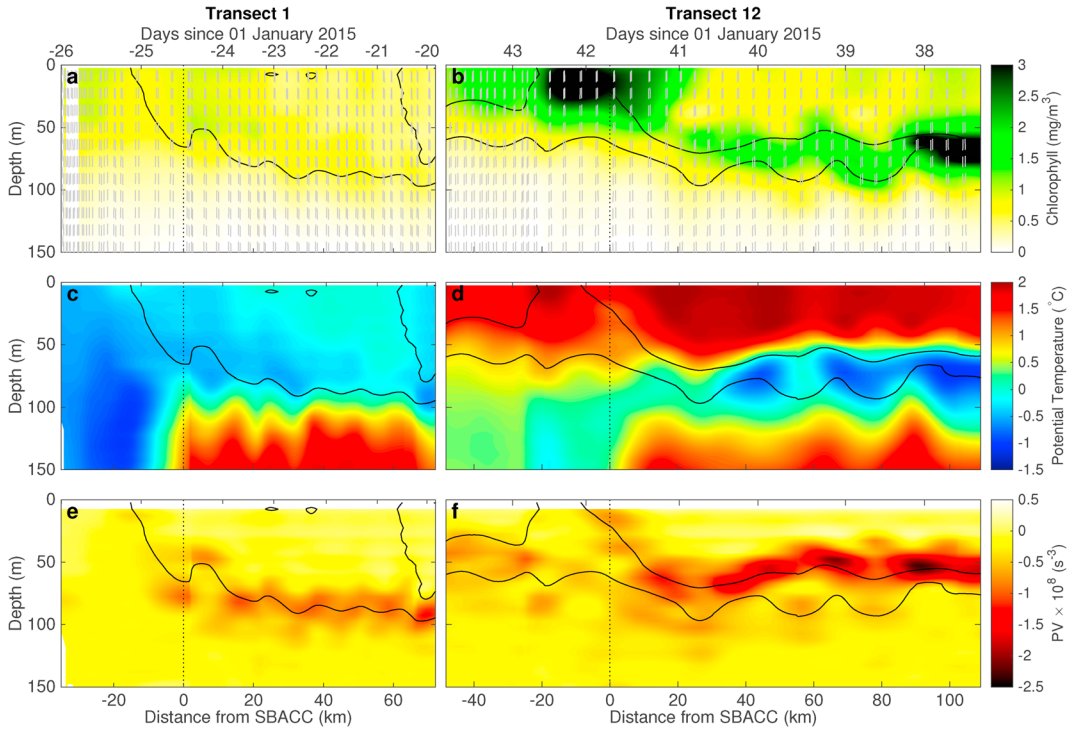

Figure 2. Winter water capping and development of an along-isopycnal PV gradient. (a, b) Objectively mapped corrected chlorophyll measurements for Transects 1 and 12. Isopycnal contours at 1027.2 and 1027.35 kg/m^3 are shown in black. Glider path is given by the grey dashed line. Distance is determined from the 2000 m isobath, where negative values are closer to the coast. (c, d) As in Figures 2a and 2b, but colors shown are potential temperature data from Transects 1 and 12. (e, f) As in Figures 2a and 2b, but colors shown are PV.

DCMs can result from an increase at depth of phytoplankters or from an increase in the chlorophyll:biomass ratio in phytoplankton at depth through photoacclimation. In Figure 1d we provide backscatter data (650 nm) from the same two transects (all transects in Figure S6). Backscatter provides a measure of the concentration of total particulate matter in the ocean and is well correlated with phytoplankton concentration in the open ocean [*Boss et al.*, 2008]. In these example transects, the combination of high fluorescence measurements and high backscatter provides strong evidence that there exists a layer of elevated phytoplankton concentration below the mixed layer.

We also consider the relation of the DCM to the euphotic layer depth, shown as the solid (1% of surface PAR) and dashed (isolume method) black lines in Figure 1e (see section 2.4; all transects in Figure S7). Both definitions show that the DCM is located below the euphotic layer, although we note that the light attenuation coefficient is strongly dependent on water column chlorophyll concentration, meaning we cannot rule out the possibility that available light may allow net photosynthesis at the top of the DCM.

3.2. Subduction Through Thickness Fluxes

In Figure 1 we highlight the isopycnal layer between 1027.2 and 1027.35 kg/m^3, which at depth is associated with the winter water (WW) layer. In spring and early summer, WW extends to the surface and stratification (lateral and vertical) is weak. Low biomass is observed throughout the region, presumably caused by light limitation (Figure 2a). The outcrop area of the WW isopycnal is large in extent and reaches off the shelf into the open ocean. As summer progresses, increasing insolation fuels an on-shelf phytoplankton bloom (Figure 2b) and warms the upper ~50 m of the water column, capping the existing WW layer (Figures 2c and 2d and all transects in Figure S9). The WW isopycnal layer deepens and thins, increasing the vertical stratification in the upper 50–70 m. The meridional extent of the WW isopycnal outcrop decreases and moves poleward onto the shelf.

A widely used ocean tracer is potential vorticity (PV), which is conserved in the ocean interior where diabatic processes are weak. In the presence of a mesoscale or submesoscale eddy field, eddy fluxes tend to reduce

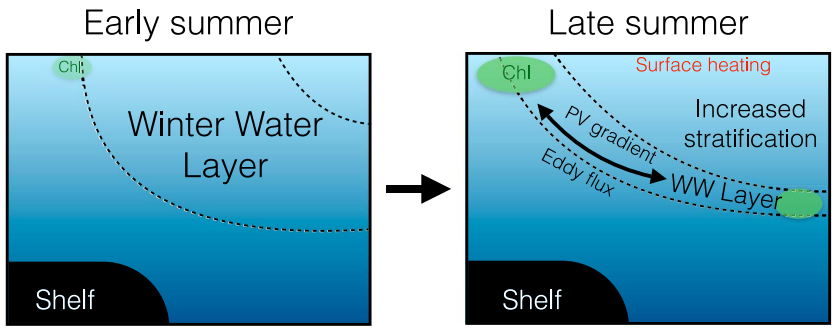

Figure 3. Schematic of mechanism generating off-shelf DCMs.

the PV gradient, homogenizing PV along isopycnal layers [*Marshall et al.*, 1993]. We approximate PV as

$$q \approx (f^2 N^2 - M^4)/f, \tag{1}$$

where f is the planetary vorticity, $N^2 = \partial_z b$ is the vertical stratification, $M^2 = \nabla_h b \approx \partial_y b$ is the horizontal stratification, ∇_h is the horizontal gradient operator, and we consider only the along-track cross-frontal component (y axis) [*Thompson et al.*, 2016]. The vertical stratification term (N^2) dominates the PV equation in most cases, although at frontal regions the horizontal stratification (M^2) becomes important.

PV (equation (1)) is shown for two transects in Figures 2e and 2f (all transects in Figure S10). An along-isopycnal gradient in PV develops in late summer just north of the SBACC. The reduction of the PV gradient is associated with an eddy thickness flux that produces an eddy velocity (defined below) transporting tracers offshore [*Marshall and Radko*, 2003]. In the case of a surface bloom, eddies will subduct high-biomass water to depth along the WW isopycnal layer (Figure 3).

4. Discussion

4.1. Scaling Arguments

We propose that eddies in our study region will produce an offshore mass transport, consistent with a down-gradient PV flux. This mechanism can be considered in two stages: vertical velocity w associated with submesoscale ageostrophic circulations in frontal regions, and along-isopycnal mixing through mesoscale motions.

We estimate w using the mixed layer restratification stream function from *Fox-Kemper et al.* [2008],

$$\psi_{ML} = \frac{C_e H^2 M^2 \mu(z)}{|f|}, \quad w = \psi_y, \tag{2}$$

where C_e is an empirically derived scaling constant, H is the mixed layer depth, and $\mu(z)$ is a dimensionless constant such that $0 \leq \mu(z) \leq 1$. Scaling arguments give

$$w \sim \frac{C_e H^2 M^2 \mu(z)}{|f| L} \sim \frac{(0.1)(50\ \mathrm{m})^2 (10^{-6}\ \mathrm{s}^{-2})(1)}{(10^{-4}\ \mathrm{s}^{-1})(10^4\ \mathrm{m})} \sim 25\ \mathrm{m/day}, \tag{3}$$

which agrees well with typical submesoscale-induced vertical velocities of $\mathcal{O}(10\ \mathrm{m/day})$ [e.g., *Levy et al.*, 2012] and gives a subduction time scale of approximately 2 days.

To estimate a time scale for mesoscale, along-isopycnal advection, we use a high-resolution (1/12°, approximately 4.5 km at this latitude) Southern Ocean model (section 2.6) to calculate the thickness-weighted velocities in the WW isopycnal layer [*Marshall and Radko*, 2003]. We directly calculate the residual velocities

$$\bar{\mathbf{u}}_{res} = \frac{\overline{\mathbf{u}h}}{\bar{h}} = \bar{\mathbf{u}} + \frac{\overline{\mathbf{u}'h'}}{\bar{h}}, \tag{4}$$

where $\mathbf{u} = (u, v)$ and primes are deviations in temporal averages (overbars), associated with a given isopycnal layer of thickness h. The total and eddy residual velocities perpendicular to the continental shelf for the isopycnal layer 1026.9–1027.1 kg/m^3 during the summer of 2008–2009 are shown in Figure 4. We choose this

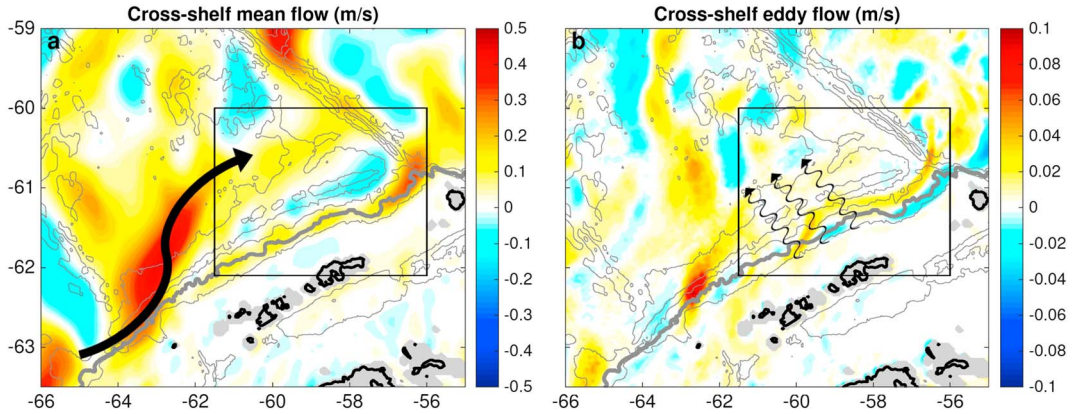

Figure 4. Layer-wise velocities from the Southern Ocean model. (a) Mean and (b) eddy residual velocities for 15 November 2007 to 15 April 2008 in the isopycnal layer 1026.9–1027.1 kg/m^3. Bathymetric contours at 1 km intervals are shown in grey (2 km bold), and black box gives domain of Figure 1a. Arrows give a general sense of the flow.

isopycnal layer because its outcrop location approximately matches that of the WW layer in our data; however, our results are not dependent on the exact isopycnal layer or the model year used.

The residual velocities are dominated by the mean term and show a meandering front that largely follows contours of constant f/H (where H is full ocean depth; Figure 4a). Large off-shelf velocities near the shelf break at 63°W are due to conservation of PV downstream of a bathymetric ridge. The total velocity also includes a large along-slope term (not shown). The eddy component, while smaller, consistently transports water off-shelf throughout this density layer (Figure 4b).

Using a characteristic eddy velocity of 0.05 m/s, we estimate that eddy-driven transport across the front could transport high-chlorophyll waters approximately 100 km offshore (Figure 1c) in about 20 days. The mean velocity transport mechanism includes a large along-slope component. Using a characteristic mean velocity of 0.2 m/s and a length of 150 km gives an estimate of mean flow transport across the front of 8 days. We expect both mean and eddy components to contribute to the offshore DCM, emphasizing the three-dimensionality of the system.

4.2. *T-S* Properties

Although the DCM lies in the same isopycnal layer as the surface bloom, the *T-S* properties are distinct. The strong frontal system in this area separates water masses, but infilling of properties is also observed, indicating the presence of small-scale, irreversible mixing (Figure 1b). Recently, *Klymak et al.* [2016] observed submesoscale-induced mixing across the Gulf Stream, where "streamers" of water masses with drawn-out *T-S* properties are subducted along isopycnals.

Klymak et al. [2016] used Lagrangian drifters to track streamers as they detrained from the Gulf Stream. Here, we use daily snapshots of salinity data along an isopycnal surface from the Southern Ocean model to suggest that streamers are also present in this region, as a strong frontal feature associated with the SBACC is present along with strong eddy activity across this front (Movie S1).

4.3. Biological Considerations

DCMs in this area have generally been attributed to biological production. *Holm-Hansen and Hewes* [2004] conclude that they are the result of positive net community production, in part due to increased oxygen concentration in DCM locations. We note that oxygen saturation is the appropriate variable due to temperature effects on solubility, and do not observe a maximum in this quantity at the depth of the DCM (Figure S11). However, the oxygen released through net community production of the scale of this DCM is small compared to the spread in oxygen measurements, and ventilation of near-surface waters through wind-driven mixing means that a large accumulation of oxygen at this depth is unlikely. Oxygen data therefore provide neither evidence for nor evidence against our hypothesis.

The DCM lies mainly below the euphotic depth and is coincident with a maxima in backscatter, suggesting that it is not simply a result of photoacclimation. The thickness of the DCM layer is greater than the typical thickness of thin phytoplankton layers (<5 m [*Dekshenieks et al.*, 2001]) and located below the pycnocline,

making it unlikely that it formed through biological settling in the water column. Another option is that biomass accumulates in the WW isopycnal layer as that layer is thinned by increased insolation and capped by warmer water through buoyancy equilibration or preferential photosynthesis in potentially iron-replete WW. An off-shelf surface bloom exists far upstream from our study region in early austral spring (Figure S4); however, this bloom does not persist into late December, when surface warming caps WW. While we do not entirely discount biological production in the DCM, the reasons above support the conclusion that an off-shelf flux of high-chlorophyll surface waters contributes significantly to the presence of the DCM in this area.

An important prediction of our hypothesis is that the ecosystem composition in the off-shelf DCM should resemble that of the on-shelf bloom, although we do not expect chlorophyll to act purely as a passive tracer and some community evolution should be anticipated [*Hood et al.*, 1991]. *Mendes et al.* [2012] conducted a chemotaxonomic HPLC (high-performance liquid chromatography) analysis on stations within our study area in February/March 2008. They note a sharp gradient in surface ecosystem composition between on-shelf and off-shelf waters. However, the ecosystem composition at depth off-shelf (60–100 m, within our DCM layer) much more closely resembles the surface community on-shelf, especially with regard to its percentage of diatoms. Diatoms tend to dominate other species in high-iron conditions [*Boyd et al.*, 2000]. While the high proportion of diatoms in the DCM can be attributed to high-iron concentrations from periodic intrusions of CDW water [*Prézelin et al.*, 2000], advection of either high-iron or high-diatom shelf waters into the area through the mechanism we propose is also consistent with these observations.

The F:b_{bp} ratio is another important biological measurement. As mentioned above, this ratio is dependent on a wide variety of factors, one of which is ecosystem community. In Figure 1f we show this ratio for Transects 11 and 12 (all transects in Figure S8). The daily cycle in the upper ~50 m is due to NPQ effects. Considering only the off-shelf area, this ratio increases with depth, as expected based on photoacclimation [*Cullen*, 1982; *Neori et al.*, 1984]. However, the similarity in this ratio between on-shelf and off-shelf blooms is consistent with our advection hypothesis.

4.4. Strength of the Biological Pump

Subduction along isopycnals acts to export material below the mixed layer and out of the euphotic zone. Net subduction therefore contributes to a flux of chlorophyll out of the productive sunlight region and below the depth of surface observations, although storms may deepen the mixed layer sufficiently to partially negate this effect (this may be present in Transect 6; see Figure S5). This mechanism suggests a chemostat-like surface environment, where surface on-shelf net primary production is partially balanced by an off-shelf flux. Estimates and models of net primary productivity that do not take into account this subduction mechanism may underestimate the strength of the biological pump in this region.

5. Conclusion

We use high-resolution Seaglider data over a period of 3 months to document the seasonal development of a PV gradient along the WW isopycnal layer. We suggest that this gradient will tend to be relaxed through the actions of eddies formed on shelf or advected into the region by the ACC and will subduct high-chlorophyll waters offshore in the WW layer. We find evidence of chlorophyll subduction along isopycnals, which is not captured in satellite imagery (Figures 1a and S4) or in climate simulations due to its small scale. This mechanism potentially functions as a highly efficient biological pump in southern Drake Passage and may be present in topographically similar areas with large surface phytoplankton blooms such as the Kerguelen and Campbell Plateau regions. This study suggests that mesoscale and submesoscale dynamics can make an important contribution to the subduction of high-biomass water masses in the Southern Ocean, emphasizing the need for parameterization in numerical models, especially in strong frontal regions.

Acknowledgments

The authors thank the captains and crews of the ARSV Laurence M. Gould and the RSS Shackleton for their assistance in the deployment and recovery of the gliders during this project. Z.K.E. and A.F.T. gratefully acknowledge funding from the David and Lucille Packard Foundation. The authors are supported by National Science Foundation (NSF) grants OPP-1246460 (Z.K.E. and A.F.T.), OPP-1246160 (J.S.), OCE-1234473 (M.R.M.), and PLR-1425989 (M.R.M.). Seaglider measurements were processed using the UEA Seaglider Toolbox (https://bitbucket.org/bastienqueste/uea-seaglider-toolbox) kindly provided by Bastien Y. Queste. Satellite data were provided by NASA Goddard Space Flight Center at http://oceancolor.gsfc.nasa.gov/. The model was run using the Extreme Science and Engineering Discovery Environment (XSEDE), which is supported by NSF grant OCE-130007. Z.K.E. would like to thank Emmanuel Boss, John Cullen, Nils Haëntjens, and Tim Smyth for valuable conversations related to this project. Seaglider data may be obtained from Z.K.E. The authors thank Tom Trull and two anonymous reviewers for their constructive reviews of this study.

References

Amante, C., and B. W. Eakins (2009), ETOPO1 1 Arc-Minute Global Relief Model: Procedures, data sources and analysis, *NOAA Tech. Memo. NESDIS NGDC-24*, 19 pp., Natl. Geophys. Data Cent., Boulder, Colo.

Arrigo, K. R., D. H. Robinson, D. L. Worthen, B. Schieber, and M. P. Lizotte (1998), Bio-optical properties of the southwestern Ross Sea, *J. Geophys. Res.*, *103*, 21,683–21,695.

Arrigo, K. R., G. L. van Dijken, and S. Bushinsky (2008), Primary production in the Southern Ocean, 1997–2006, *J. Geophys. Res.*, *113*, C08004, doi:10.1029/2007JC004551.

Banse, K. (2004), Should we continue to use the 1% light depth convention for estimating the compensation depth of phytoplankton for another 70 years?, *Limnol. Oceanogr. Bull.*, *13*, 49–52.

Behrenfeld, M. J., and P. G. Falkowski (1997), Photosynthetic rates derived from satellite-based chlorophyll concentration, *Limnol. Oceanogr.*, *42*, 1–20.

Boss, E., D. Swift, L. Taylor, P. Brickley, R. Zaneveld, S. Riser, M. J. Perry, and P. G. Strutton (2008), Observations of pigment and particle distributions in the western North Atlantic from an autonomous float and ocean color satellite, *Limnol. Oceanogr.*, *53*, 2112–2122.

Boss, E. B., and N. Haëntjens (2016), Primer regarding measurements of chlorophyll fluorescence and the backscattering coefficient with WETLabs FLBB on profiling floats, *SOCCOM Tech. Rep. 2016-1*. [Available at http://soccom.princeton.edu/sites/default/files/files/SOCCOM_2016-1_Bio-optics-primer.pdf.]

Boyd, P. W., and M. J. Ellwood (2010), The biogeochemical cycle of the ocean, *Nat. Geosci.*, *3*, 675–682, doi:10.1038/ngeo964.

Boyd, P. W., et al. (2000), A mesoscale phytoplankton bloom in the polar Southern Ocean stimulated by iron fertilization, *Nature*, *407*, 695–702, doi:10.1038/35037500.

Broecker, W. S., et al. (1998), How much deep water is formed in the Southern Ocean?, *J. Geophys. Res.*, *103*, 15,833–15,843.

Carr, M., et al. (2006), A comparison of global estimates of marine primary production from ocean color, *Deep Sea Res., Part II*, *53*, 741–770, doi:10.1016/j.dsr2.2006.01.028.

Cassar, N., P. J. DiFiore, B. A. Barnett, M. L. Bender, A. R. Bowie, B. Tilbrook, K. Petrou, K. J. Westwood, S. W. Wright, and D. Lefevre (2011), The influence of iron and light on net community production in the Subantarctic and Polar Frontal Zones, *Biogeosciences*, *8*, 227–237, doi:10.5194/bg-8-227-2011.

Cullen, J. J. (1982), The deep chlorophyll maximum: Comparing vertical profiles of chlorophyll a, *Can. J. Fish. Aquat. Sci.*, *39*, 791–803.

Cullen, J. J. (2015), Subsurface chlorophyll maximum layers: Enduring enigma or mystery solved?, *Annu. Rev. Mar. Sci.*, *7*, 207–239, doi:10.1146/annurev-marine-010213-135111.

Cullen, J. J., and M. R. Lewis (1995), Biological processes and optical measurements near the sea surface: Some issues relevant to remote sensing, *J. Geophys. Res.*, *100*, 13,255–13,266.

Dekshenieks, M. M., P. L. Donaghay, J. M. Sullivan, J. E. B. Rines, T. R. Osborn, and M. S. Twardowski (2001), Temporal and spatial occurrence of thin phytoplankton layers in relation to physical processes, *Mar. Ecol. Prog. Ser.*, *223*, 61–71.

Dong, S., J. Sprintall, S. T. Gille, and L. Talley (2008), Southern Ocean mixed-layer depth from Argo float profiles, *J. Geophys. Res.*, *113*, C06013, doi:10.1029/2006JC004051.

Dulaiova, H., M. V. Ardelan, P. B. Henderson, and M. A. Charette (2009), Shelf-derived iron inputs drive biological productivity in the southern Drake Passage, *Global Biogeochem. Cycles*, *23*, GB4014, doi:10.1029/2008GB003406.

Dunne, J. P., A. Armstrong, A. Gnanadesikan, and J. L. Sarmiento (2005), Empirical and mechanistic models for the particle export ratio, *Global Biogeochem. Cycles*, *19*, GB4026, doi:10.1029/2004GB002390.

Field, C. B., M. J. Behrenfeld, J. T. Randerson, and P. Falkowski (1998), Primary production of the biosphere: Integrating terrestrial and oceanic components, *Science*, *281*, 237–240, doi:10.1126/science.281.5374.237.

Fox-Kemper, B., R. Ferrari, and R. Hallberg (2008), Parameterization of mixed layer eddies. Part I: Theory and diagnosis, *J. Phys. Oceanogr.*, *38*, 1145–1165, doi:10.1175/2007JPO3792.1.

Frants, M., S. T. Gille, M. Hatta, W. T. Hiscock, M. Kahru, C. I. Measures, B. G. Mitchell, and M. Zhou (2013), Analysis of horizontal and vertical processes contributing to natural iron supply in the mixed layer in southern Drake Passage, *Deep Sea Res., Part II*, *90*, 68–76, doi:10.1016/j.dsr2.2012.06.001.

Frenger, I., M. Münnich, N. Gruber, and R. Knutti (2015), Southern Ocean eddy phenomenology, *J. Geophys. Res. Oceans*, *120*, 7413–7449, doi:10.1002/2015JC011047.

Gordon, H. R., and W. R. McCluney (1975), Estimation of the depth of sunlight penetration in the sea for remote sensing, *Appl. Opt.*, *14*, 413–416.

Gruber, N., et al. (2009), Oceanic sources, sinks, and transport of atmospheric CO_2, *Global Biogeochem. Cycles*, *22*, GB1005, doi:10.1029/2008GB003349.

Holm-Hansen, O., and C. D. Hewes (2004), Deep chlorophyll-a maxima (DCMs) in Antarctic waters. I. Relationships between DCMs and the physical, chemical, and optical conditions in the upper water column, *Polar Biol.*, *27*, 699–710, doi:10.1007/s00300-004-0641-1.

Holm-Hansen, O., and B. G. Mitchell (1991), Spatial and temporal distribution of phytoplankton and primary production in the western Bransfield Strait region, *Deep Sea Res.*, *38*, 961–980.

Holm-Hansen, O., M. Kahru, and C. D. Hewes (2005), Deep chlorophyll a maxima (DCMs) in pelagic Antarctic waters. II. Relation to bathymetric features and dissolved iron concentrations, *Mar. Ecol. Prog. Ser.*, *297*, 71–81.

Hood, R. R., M. R. Abbott, and A. Huyer (1991), Phytoplankton and photosynthetic light response in the coastal transition zone off northern California in June 1987, *J. Geophys. Res.*, *96*, 14,769–14,780.

Johnson, R., P. G. Strutton, S. W. Wright, A. McMinn, and K. M. Meiners (2013), Three improved satellite chlorophyll algorithms for the Southern Ocean, *J. Geophys. Res. Oceans*, *118*, 3694–3703, doi:10.1002/jgrc.20270.

Kadko, D. C., L. Washburn, and B. Jones (1991), Evidence of subduction within cold filaments of the northern California Coastal Transition Zone, *J. Geophys. Res.*, *96*, 14,909–14,926.

Kahru, M., and B. G. Mitchell (2010), Blending of ocean colour algorithms applied to the Southern Ocean, *Remote Sens. Lett.*, *1*, 119–124, doi:10.1080/01431160903547940.

Klymak, J. M., et al. (2016), Submesoscale streamers exchange water on the north wall of the Gulf Stream, *Geophys. Res. Lett.*, *43*, 1226–1233, doi:10.1002/2015GL067152.

Lapeyre, G., P. Klein, and B. L. Hua (2006), Oceanic restratification forced by surface frontogenesis, *J. Phys. Oceanogr.*, *36*, 1577–1590, doi:10.1175/JPO2923.1.

Large, W. G., and S. G. Yeager (2004), Diurnal to decadal global forcing for ocean and sea-ice models: The data sets and flux climatologies, *NCAR Tech. Rep. TN-4601STR*, 112 pp., NCAR, Boulder, Colo.

Levy, M., R. Ferrari, P. J. S. Franks, A. P. Martin, and P. Rivière (2012), Bringing physics to life at the submesoscale, *Geophys. Res. Lett.*, *39*, L14602, doi:10.1029/2012GL052756.

Longhurst, A. R., and W. G. Harrison (1989), The biological pump: Profiles of plankton production and consumption in the upper ocean, *Prog. Oceanogr.*, *22*, 47–123, doi:10.1016/0079-6611(89)90010-4.

Mahadevan, A., and A. Tandon (2006), An analysis of mechanisms for submesoscale vertical motion at ocean fronts, *Ocean Modell.*, *14*, 241–256, doi:10.1016/j.ocemod.2006.05.006.

Marshall, J., and T. Radko (2003), Residual-mean solutions for the Antarctic Circumpolar Current and its associated overturning circulation, *J. Phys. Oceanogr.*, *33*, 2341–2354.

Marshall, J., D. Olbers, H. Ross, and D. Wolf-Gladrow (1993), Potential vorticity constraints on the dynamics and hydrography of the Southern Ocean, *J. Phys. Oceanogr.*, *23*, 465–487.

Marshall, J., A. Adcroft, C. Hill, L. Perelman, and C. Heisey (1997), A finite-volume, incompressible Navier Stokes model for studies of the ocean on parallel computers, *J. Geophys. Res.*, *102*, 5753–5766, doi:10.1029/96JC02775.
Martin, J. H. (1990), Glacial-interglacial CO_2 change: The iron hypothesis, *Paleoceanography*, *5*, 1–13.
Martin, J. H., R. M. Gordon, and S. E. Fitzwater (1990), Iron in Antarctic waters, *Nature*, *345*, 156–158, doi:10.1038/345156a0.
Mazloff, M. R., P. Heimbach, and C. Wunsch (2010), An eddy-permitting Southern Ocean state estimate, *J. Phys. Oceanogr.*, *40*, 880–899, doi:10.1175/2009JPO4236.1.
Measures, C. I., M. T. Brown, K. E. Selph, A. Apprill, M. Zhou, M. Hatta, and W. T. Hiscock (2013), The influence of shelf processes in delivering dissolved iron to the HNLC waters of the Drake Passage, Antarctica, *Deep Sea Res., Part II*, *90*, 77–88, doi:10.1016/j.dsr2.2012.11.004.
Mendes, C. R. B., M. S. de Souza, V. M. T. Garcia, M. C. Leal, V. Brotas, and C. A. E. Garcia (2012), Dynamics of phytoplankton communities during late summer around the tip of the Antarctic Peninsula, *Deep Sea Res., Part I*, *65*, 1–14, doi:10.1016/j.dsr.2012.03.002.
Mitchell, B. G., and O. Holm-Hansen (1991), Bio-optical properties of Antarctic Peninsula waters: Differentiation from temperate ocean models, *Deep Sea Res.*, *38*, 1009–1028.
Mitchell, B. G., E. A. Brody, O. Holm-Hansen, C. McClain, and J. Bishop (1991), Light limitation of phytoplankton biomass and macronutrient utilization in the Southern Ocean, *Limnol. Oceanogr.*, *36*, 1662–1677, doi:10.4319/lo.1991.36.8.1662.
Neori, A., O. Holm-Hansen, B. G. Mitchell, and D. A. Kiefer (1984), Photoadaptation in marine phytoplankton, *Plant Physiol.*, *76*, 518–524.
Omand, M. M., E. A. D'Assaro, C. M. Lee, M. J. Perry, N. Briggs, I. Cetinić, and A. Mahadevan (2015), Eddy-driven subduction exports particulate organic carbon from the spring bloom, *Science*, *348*, 222–225, doi:10.1126/science.1260062.
Orsi, A. H., T. Whitworth, and W. D. Nowlin Jr. (1995), On the meridional extent and fronts of the Antarctic Circumpolar Current, *Deep Sea Res., Part I*, *42*, 641–673.
Prézelin, B. B., E. E. Hofmann, C. Mengelt, and J. M. Klinck (2000), The linkage between Upper Circumpolar Deep Water (UCDW) and phytoplankton assemblages on the west Antarctic Peninsula continental shelf, *J. Mar. Res.*, *58*, 165–202.
Ralston, D. K., D. J. McGillicuddy Jr., and D. W. Townsend (2007), Asynchronous vertical migration and bimodal distribution of motile phytoplankton, *J. Plankton Res.*, *29*, 803–821, doi:10.1093/plankt/fbm061.
Richardson, T. L., and J. J. Cullen (1995), Changes in buoyancy and chemical composition during the growth of a coastal marine diatom: Ecological and biogeochemical consequences, *Mar. Ecol. Prog. Ser.*, *128*, 77–90.
Rosso, I., A. M. Hogg, P. G. Strutton, A. E. Kiss, R. Matear, A. Klocker, and E. van Sebille (2014), Vertical transport in the ocean due to sub-mesoscale structures: Impacts in the Kerguelen region, *Ocean Modell.*, *80*, 10–23, doi:10.1016/j.ocemod.2014.05.001.
Rosso, I., A. M. Hogg, A. E. Kiss, and B. Gayen (2015), Topographic influence on submesoscale dynamics in the Southern Ocean, *Geophys. Res. Lett.*, *42*, 1139–1147, doi:10.1002/2014GL062720.
Ryther, J. H. (1956), Photosynthesis in the ocean as a function of light intensity, *Limnol. Oceanogr.*, *1*, 61–70.
Sarmiento, J. L., and J. R. Toggweiler (1984), A new model for the role of the oceans in determining atmospheric pCO_2, *Nature*, *308*, 621–624.
Slovacek, R. E., and P. J. Hannan (1977), In vivo fluorescence determinations of phytoplankton chlorophyll a, *Limnol. Oceanogr.*, *22*, 919–925, doi:10.4319/lo.1977.22.5.0919.
Sokolov, S., and S. R. Rintoul (2009), Circumpolar structure and distribution of the Antarctic Circumpolar Current fronts: 1. Mean circumpolar paths, *J. Geophys. Res.*, *114*, C11018, doi:10.1029/2008JC005108.
Stacey, M. T., M. A. McManus, and J. V. Steinbuck (2007), Convergences and divergences and thin layer formation and maintenance, *Limnol. Oceanogr.*, *52*, 1523–1532.
Thompson, A. F., P. H. Haynes, C. Wilson, and K. J. Richards (2010), Rapid Southern Ocean front transitions in an eddy-resolving ocean GCM, *Geophys. Res. Lett.*, *37*, L23602, doi:10.1029/2010GL045386.
Thompson, A. F., A. Lazar, C. Buckingham, A. V. Naveira Garabato, G. M. Damerell, and K. J. Heywood (2016), Open-ocean submesoscale motions: A full seasonal cycle of mixed layer instabilities form gliders, *J. Phys. Oceanogr.*, *46*, 1285–1307, doi:10.1175/JPO-D-15-0170.1.
Washburn, L., D. C. Kadko, B. H. Jones, T. Hayward, P. M. Kosro, T. P. Stanton, S. Ramp, and T. Cowles (1991), Water mass subduction and the transport of phytoplankton in a coastal upwelling system, *J. Geophys. Res.*, *96*, 14,927–14,945.
Weston, K., L. Fernand, D. K. Mills, R. Deahunty, and J. Brown (2005), Primary production in the deep chlorophyll maximum of the central North Sea, *J. Plankton Res.*, *27*, 909–922, doi:10.1093/plankt/fbi064.
Zhou, M., Y. Zhu, R. Dorland, and C. I. Measures (2010), Dynamics of the current system in the southern Drake Passage, *Deep Sea Res., Part I*, *57*, 1039–1048, doi:10.1016/j.dsr.2010.05.012.